Soft magnetic properties and giant magneto-impedance effect of Fe-Zr-Nb-B-Cu ribbons

1999 J. Phys.: Condens. Matter 11 4251

(http://iopscience.iop.org/0953-8984/11/21/311)

J. Phys.: Condens. Matter **11** (1999) 4251–4259. Printed in the UK PII: S0953-8984(99)00692-X

Soft magnetic properties and giant magneto-impedance effect of Fe–Zr–Nb–B–Cu ribbons

J He†‡, H Q Guo†, B G Shen†, K Y He‡ and J F Hu§

† State Key Laboratory of Magnetism, Institute of Physics and Centre for Condensed Matter Physics, Chinese Academy of Sciences, Beijing 100080, People's Republic of China
‡ Department of Material Sciences and Engineering, Northeastern University, Shenyang 110006, People's Republic of China
§ Department of Physics, Shandong University, Jinan 250100, People's Republic of China

Received 5 January 1999, in final form 22 March 1999

Abstract. The soft magnetic properties and the giant magneto-impedance (GMI) effect have been studied in $Fe_{84}Zr_{3.5}Nb_{3.5}B_8Cu$ ribbons. The annealed samples with nanocrystalline structure show excellent soft magnetic properties and induced transverse anisotropy. The effective permeability is found to reach a maximum for the sample annealed at 923 K for 20 min. The maximal magneto-impedance ratio $\Delta Z/Z$ ($\Delta Z/Z = (Z(H) - Z(H_{max}))/Z(H_{max})$) of about 383% and the maximal sensitivity (i.e. the maximal value of the derivative of the $\Delta Z/Z$–H_L curve) of about 0.91% (A $m^{-1})^{-1}$ (72% Oe^{-1}) are measured at frequency $f = 2.5$ MHz for the same sample. The excellent soft magnetic properties and the induced transverse anisotropy are the basis of obtaining the sensitive magneto-impedance response. The intrinsic mechanism of the influence of the soft magnetic properties on the GMI effect is discussed briefly.

1. Introduction

The GMI effect is a phenomenon of electromagnetic induction in which the voltage $V = RI + V_L$ (V_L is inductive voltage) induced by a high-frequency current for magnetic materials changes with the application of a moderate dc field H_L. At the low-frequency range of 1–10 kHz, the change of V is due to the decrease of the internal inductance L_i by the transverse magnetization. This is the magnetic-inductive effect. At the high-frequency range, the skin effect is so strong that the current is distributed near the surface of materials. The change of V results from the variation of both the resistive and inductive components of impedance Z, which is associated with the decrease of circular permeability for wires or transverse permeability for ribbons owing to the application of the longitudinal dc field H_L. The sensitive change of V or Z is called the GMI effect [1].

Previous reports have indicated that the soft magnetic materials, such as Co-based amorphous wires [2, 3], ribbons [4] and Fe-based nanocrystalline ribbons [5–8] and films [9], possess considerable GMI response. The excellent soft magnetic properties of lower magnetostriction and higher permeability along with the circular or transverse anisotropy are the main premise to the GMI response. Recently, Makino *et al* [10] found that the coexistence of Zr and Nb in the Fe–M–B based alloys allows access to the realization of forming nearly zero magnetostriction materials, leading to obvious improvement of the soft magnetic properties. This development of the new soft magnetic nanocrystalline alloys with the excellent characteristics of high saturation magnetic induction B_s above 1.5 T and effective permeability

0953-8984/99/214251+09$19.50

μ' above 10^5 predicts a comprehensive application prospect in the fields of power transformers, magnetic heads, magnetic sensors and so on. In this paper, in combination with the research on the primary crystallization, nanostructure and soft magnetic properties, the GMI effect of the $Fe_{84}Zr_{3.5}Nb_{3.5}B_8Cu$ alloys is first reported in detail. The influence of the soft magnetic properties on the GMI effect was observed through the sharp contrast of the amorphous sample and the nanocrystalline samples. By properly optimizing the soft magnetic properties, it will be possible to tailor the $Fe_{84}Zr_{3.5}Nb_{3.5}B_8Cu$ alloys to fit specific applications.

2. Experimental procedures

As-quenched (AQ) amorphous ribbons $Fe_{84}Zr_{3.5}Nb_{3.5}B_8Cu$ were prepared by the standard melt-spinning technique. Surface velocity of the Cu wheel around 35 m s^{-1} was used to avoid the appearance of texture in the samples. Ribbons 20 μm in thick and 1.2 mm in width were cut to 50 mm in length, and then annealed at different temperatures from 723 K to 973 K for 20 min in a vacuum of 5×10^{-3} Pa. All the samples were naturally cooled at room temperature without magnetic field. With the program control, the power-compensation technique was used to determine the primary crystallization behaviour in an advanced CDR-1 differential scanning calorimeter (DSC). The DSC curve was determined by the heat flow ratio dh/dT as well as the power difference ΔW between the samples and the reference test powder Al_2O_3 (dh/dT is used as ordinate and the heating temperature as abscissa). X-ray diffraction (XRD) was used to identify the crystallographic structure. The XRD measurement was carried out in a standard Philips PW 1820 Bragg–Brentano diffractometer using Cu Kα radiation. The longitudinal magnetization curves and the M–H characteristic loops were obtained in an earth-field compensated solenoid using a Förster coercimeter. The values of the intrinsic coercive force H_c were determined from the M–H characteristic loops. The effective permeability μ' and the magneto-impedance of the samples were measured using the impedance analyser. Four probes made of metal Cu were symmetrically attached to the ribbons by silver glue. The contact resistance was less than 1 Ω. The drive current amplitude was 10 mA. A dc magnetic field up to 2400 A m^{-1} was applied parallel to the long axis direction of the samples using a long solenoid system. All of the data were collected at room temperature.

3. Results and discussion

3.1. Primary crystallization and nanostructure

Figure 1 shows the DSC curves of the amorphous and annealed $Fe_{84}Zr_{3.5}Nb_{3.5}B_8Cu$ ribbons with a scanning rate of 10 K s^{-1}. It is clearly found that a narrow and high exothermic peak is shown for amorphous samples. With increasing annealing temperature T_a, the exothermic peaks turn out to be wider and lower. When $T_a \geqslant 823$ K, the DSC curves are nearly straight lines, which means that the primary crystallization of the amorphous samples has finished. The measured values of the primary crystallization temperature T_{x1} for onset, T_{x2} for peaks as shown in figure 1, the crystallization enthalpies ΔH and the crystalline weight fraction w are listed in table 1. The almost fixed values of T_{x1} and T_{x2} for the amorphous and partially crystallized samples indicate that these samples have the same crystallization behaviour and the amorphous matrix has the same thermal stability. With increasing annealing temperature, the crystallization enthalpies ΔH gradually drop to zero. In order to determine the microstructure of the annealed samples, x-ray diffraction was also carried out. The XRD patterns are shown in figure 2. The typical three diffractory peaks of α-Fe bcc phase are observed for annealing temperature larger than 823 K. The results are consistent with the DSC analysis data. By means

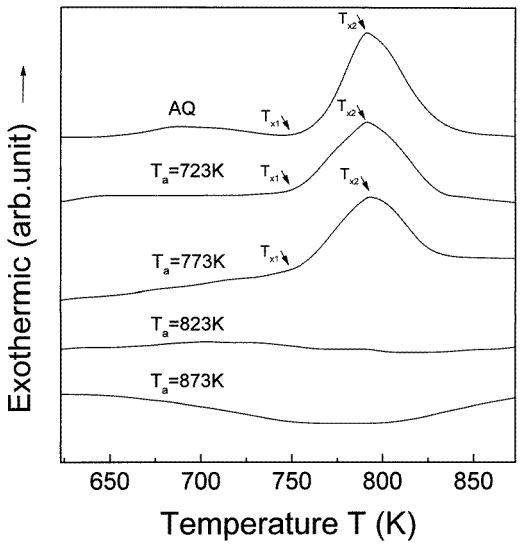

Figure 1. The DSC analysis curves of the amorphous and annealed $Fe_{84}Zr_{3.5}Nb_{3.5}B_8Cu$ ribbons.

Table 1. The DSC analysis data of the as-quenched and annealed $Fe_{84}Zr_{3.5}Nb_{3.5}B_8Cu$ ribbons.

Samples		T_{x1} (K)	T_{x2} (K)	S (mm^2)	ΔH (J G^{-1})	w (%)[a]
AQ		760	790	620	45.13	0
Annealed	723 K	758	788	510	43.07	4.58
	773 K	756	790	420	35.46	21.42
	823 K	0	0	0	0	100
	873 K	0	0	0	0	100

[a] $w = (1-\Delta H(\text{ann})/\Delta H(\text{AQ}))\%$, where $\Delta H(\text{AQ})$ and $\Delta H(\text{ann})$ are the crystallization enthalpies of the AQ and annealed $Fe_{84}Zr_{3.5}Nb_{3.5}B_8Cu$ ribbons, respectively.

of Scherrer's formula, the grain size of the samples annealed from 823 K to 923 K rises slightly from about 9 to 9.5 nm. This indicates that a superfine nanocrystalline structure is formed in $Fe_{84}Zr_{3.5}Nb_{3.5}B_8Cu$ ribbons.

3.2. Soft magnetic properties

Figure 3 shows the longitudinal magnetization curves and M–H characteristic loops for $Fe_{84}Zr_{3.5}Nb_{3.5}B_8Cu$ ribbons annealed at different temperatures. As can be seen from figure 3, all of the six annealed ribbons possess the characteristics of lower remanence and coercive force compared with those of FeZrBCu ribbons [8]. With increasing annealing temperature, the M–H loops change gradually from nonlinear to nearly linear characteristics. Such linear M–H characteristics are consistent with a pure rotational magnetization. This illustrates that the annealing treatment promotes the elimination of internal stress and induces a transverse anisotropy with respect to applied field H_a direction. The influence of the annealing temperature on the coercive force of the studied ribbons is presented in figure 4. It can be seen that for annealing temperature below that of the onset of crystallization, the coercive force is very low. This is the result of structure relaxation of the amorphous alloys. For slightly higher temperature larger than 760 K, an increase of the coercive force H_c is observed. From table 1, it is known that the weight fraction w of primary crystallization is very low at the onset

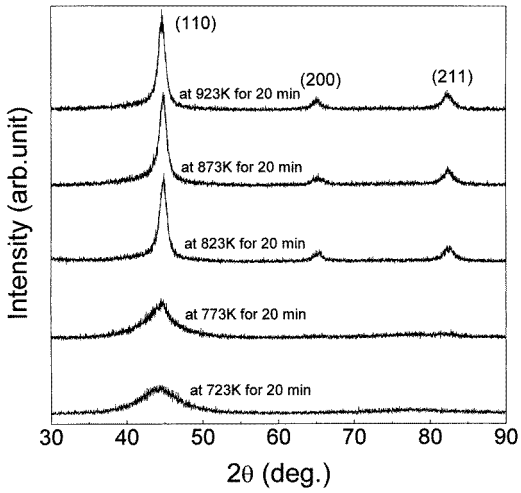

Figure 2. The x-ray diffraction patterns of the annealed $Fe_{84}Zr_{3.5}Nb_{3.5}B_8Cu$ ribbons.

of the crystallization. The average distance between the α-Fe crystallites is much larger than the exchange correlation length [11] between them. This means that the crystallites cannot be exchange coupled and the macroscopic magneto-crystalline anisotropy cannot be averaged out. This leads to the increase of the coercive force H_c. When T_a is larger than 773 K, the weight fraction rises obviously. The average distance between the nanocrystals is lower than the exchange correlation length and the magnetocrystalline anisotropy was gradually averaged out. Therefore, the coercive force H_c drops. Further increase of annealing temperature above 923 K may cause the growth of α-Fe grains and the appearance of $Fe_2(Zr, B) + Fe_3(Zr, B)$ as depicted in [12], which results in increase of the H_c again.

The curves of the effective permeability μ' versus the external longitudinal dc field H_L were also measured. As shown in figure 5, μ' of the sample annealed at 723 K is lower than those of the other samples and drops sharply only at the lower external field H_L. When annealing temperature is larger than 723 K, α-Fe bcc phase appears in the amorphous matrix. The values of μ' decline rather slowly with H_L at first, then drop dramatically at about 160 A m^{-1} and finally saturate, showing the typical property of transverse anisotropy. Furthermore, it is found that the largest effective permeability appears at $T_a = 923$ K, where the coercive force H_c reaches the minimum as shown in figure 4. Figure 6 depicts the influence of the frequency on the effective permeability μ'. It also shows that the maximal value μ' appears in the sample annealed at $T_a = 923$ K. All the curves decrease sharply in the low-frequency region (<2 MHz) and then reach saturation in the high-frequency region. The lower values of μ' at higher frequency is due to the damping force induced by eddy currents, which can limit the displacement of domain walls. The above analysis of the soft magnetic properties proves that the ribbon annealed at 923 K for 20 min possesses the best soft magnetic properties.

3.3. Magneto-impedance response

The measurements of the magneto-impedance for the amorphous and nanocrystalline samples were carried out in the external longitudinal dc field H_L from 0 to 2400 A m^{-1} for several frequencies. The GMI ratio denotes $\Delta Z/Z$ ($\Delta Z/Z = (Z(H) - Z(H_{max}))/Z(H_{max})$),

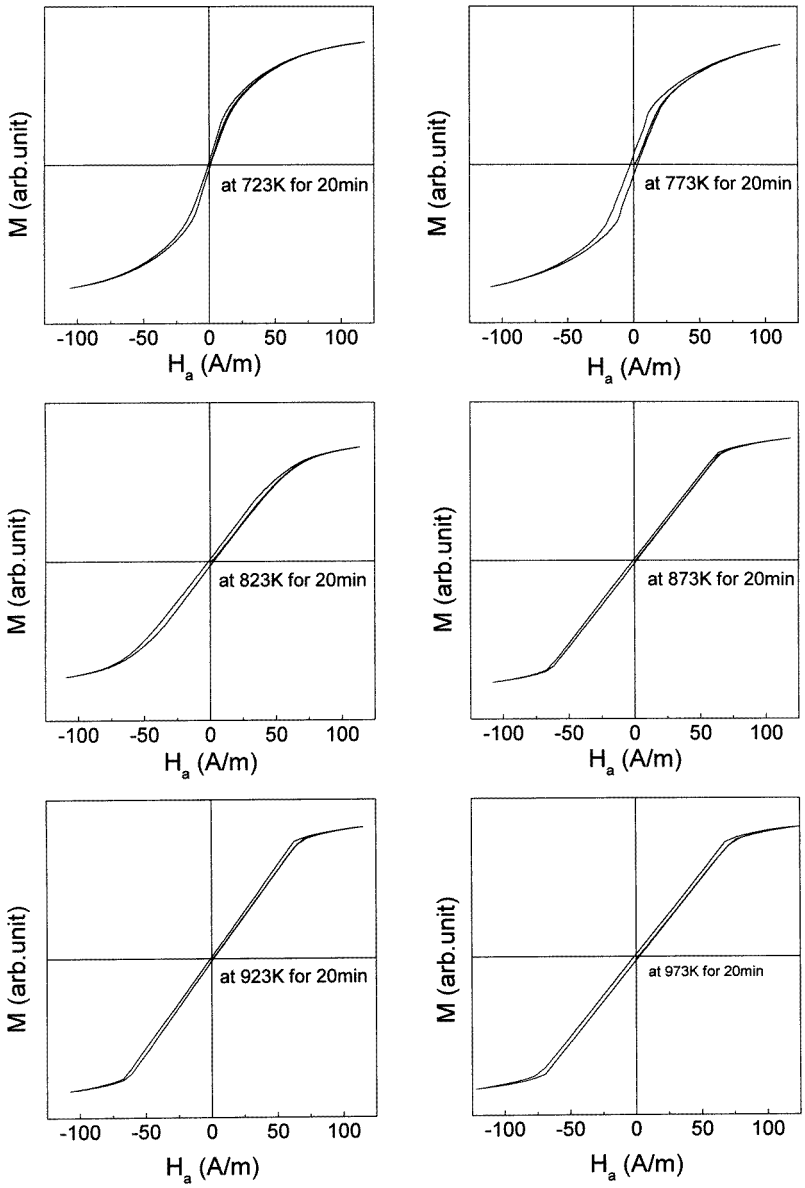

Figure 3. The M–H magnetization curves and hysteresis loops of $Fe_{84}Zr_{3.5}Nb_{3.5}B_8Cu$ ribbons.

where $Z(H_{max})$ is the impedance under the maximal external field. Figure 7 shows the field dependence of the GMI ratio of $Fe_{84}Zr_{3.5}Nb_{3.5}B_8Cu$ ribbons. For the AQ sample and that of annealed at 723 K, the GMI ratios decline slowly with increasing H_L; no obvious GMI response can be observed. For the annealed samples with nanocrystalline structure, the GMI ratios rise at first with H_L and reach the maximum $(\Delta Z/Z)_{max}$ which is located at about 60 A m^{-1}, then decrease sharply with further increasing H_L. As mentioned above in section 3.2, a transverse anisotropy is induced in the nanocrystalline samples annealed at $T_a > 723$ K. It is known that the effect of ordering alignment of the atomic pair orientation produced

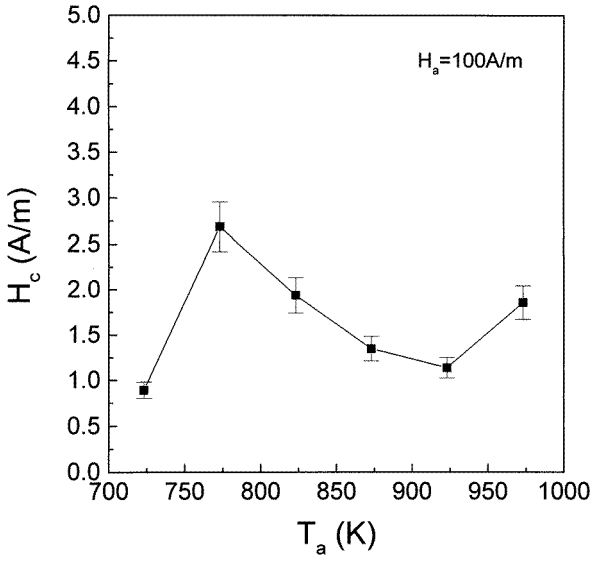

Figure 4. The dependence of coercive force H_c on the annealing temperature T_a.

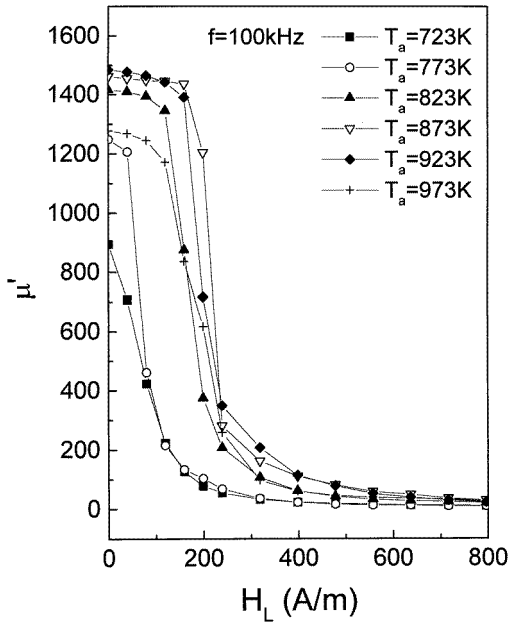

Figure 5. The dependence of effective permeability μ' of the $Fe_{84}Zr_{3.5}Nb_{3.5}B_8Cu$ ribbons annealed at different temperatures on the external longitudinal field H_L.

during the annealing process results in the induced transverse anisotropy H_k. The transverse direction becomes the easy magnetization axis. For moderate frequency, the field h ($h = I/2t$, where t is the thickness of the ribbon) induced by ac current $I = I_0 \exp(-i\omega t)$ promotes the transverse magnetization via the wall displacement of the shell domain for the characteristic core–shell domain structure [13]. The impedance responds to the magnetization process via

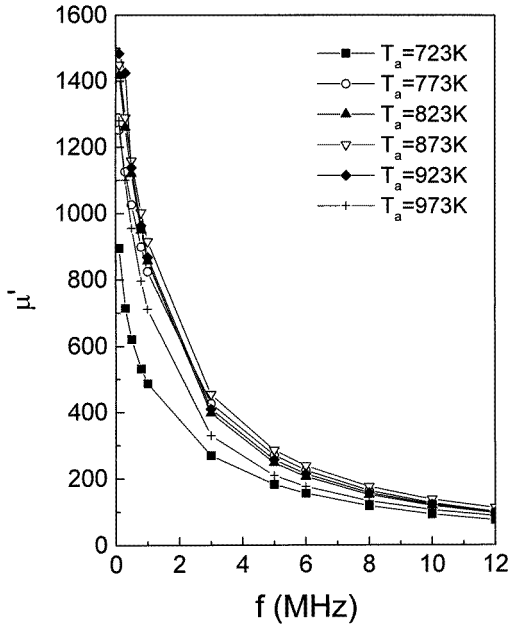

Figure 6. The dependence of effective permeability μ' of the $Fe_{84}Zr_{3.5}Nb_{3.5}B_8Cu$ ribbons annealed at different temperatures on the ac frequency f.

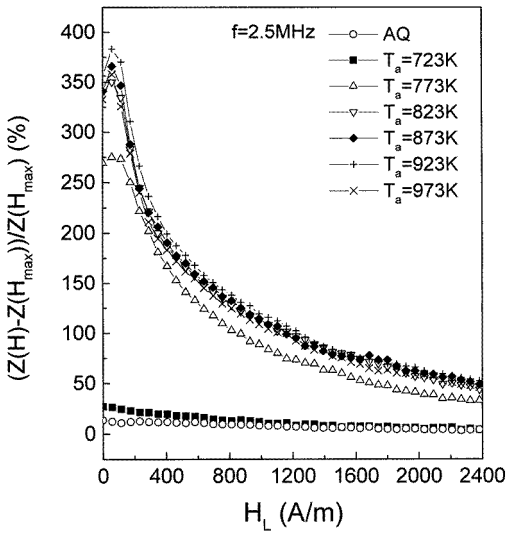

Figure 7. The curves of GMI ratio ($\Delta Z/Z$) versus external longitudinal field H_L at ac frequency 2.5 MHz for the annealed $Fe_{84}Zr_{3.5}Nb_{3.5}B_8Cu$ ribbons.

the penetration depth δ_m (see the formula (1)). When the field H_L, which is a hard axis field, is applied along the long direction of samples, the transverse magnetization via wall displacement is suppressed. The moment rotation magnetization enhances gradually. After H_L reaches and surpasses the transverse anisotropy field H_k, the effective permeability μ' drops dramatically

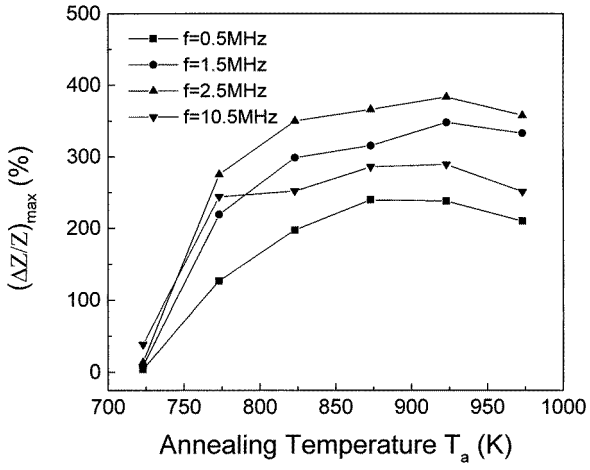

Figure 8. The dependence of the maximal GMI ratio $(\Delta Z/Z)_{max}$ on the annealing temperature T_a for different frequencies.

as shown in figure 5. Above all, for the excellent soft magnetic material, the response of μ' is more pronounced. For the sample annealed at 923 K for 20 min, the sensitivity of μ' response is about 13 $(\mathrm{A\ m^{-1}})^{-1}$ (i.e. 1040 $\mathrm{Oe^{-1}}$). Correspondingly, the GMI ratio $\Delta Z/Z$ shows the maximal value 383% at $H_L = H_k$ and the sensitivity of $\Delta Z/Z$ is about 0.91% $(\mathrm{A\ m^{-1}})^{-1}$ (72% $\mathrm{Oe^{-1}}$). This GMI effect is superior to those of Fe–Zr–B–Cu ribbons in our previous report [8]. This is because of the higher effective permeability and lower coercive force for the annealed $Fe_{84}Zr_{3.5}Nb_{3.5}B_8Cu$ ribbons, which are beneficial to the wall motion and the moment rotation. The detailed examination of the influence of transverse anisotropy on the GMI effect for the $Fe_{84}Zr_{3.5}Nb_{3.5}B_8Cu$ ribbons is under way.

Figure 8 shows the dependence of the largest GMI ratio $(\Delta Z/Z)_{max}$ on the annealing temperature T_a. It is obvious that the largest GMI effect occurs at frequency $f = 2.5$ MHz for all the annealing temperatures. The maximal values for the four curves almost appear at $T_a = 923$ K. Combined with figures 4–6, this proves again that the sample with the optimal soft magnetic properties will display the largest GMI effect.

According to the classical electromagnetism, the measured data of impedance $Z(\omega, H_L)$ change with the frequency f and the application of a longitudinal field H_L as a result of the skin effect, in conjunction with the transverse magnetization. For the simple geometry of a ribbon, the expression of Z is [14, 15]:

$$\begin{aligned} Z &= (1 - \mathrm{i})\rho L/(2d\delta_m) \\ \delta_m &= (\rho/(\pi f \mu'))^{1/2} \end{aligned} \tag{1}$$

where L and d are the length and width of the ribbon respectively and ρ is the resistivity of the sample. Formula (1) shows that the behaviour of Z is determined by the skin effect, and the impedance is proportional to the factor $(f\mu')^{0.5}$. This means that the GMI effect is subject to the mutual influence of the longitudinal field and the frequency. Only at moderate frequency can the factor $(f\mu')^{0.5}$ show a maximum. This is the reason that the best GMI effect appears at $f = 2.5$ MHz as shown in figure 8. For higher frequency larger than 2.5 MHz, the μ' drops and tends to a lower value owing to the strong eddy effect. Therefore, the GMI effect declines.

4. Conclusion

The soft magnetic properties and the GMI effect of AQ and annealed $Fe_{84}Zr_{3.5}Nb_{3.5}B_8Cu$ ribbons have been studied. The results can be summarized as follows:

(1) Superfine nanocrystalline structure (average grain size of about 9 nm) in the annealed $Fe_{84}Zr_{3.5}Nb_{3.5}B_8Cu$ ribbons is formed. The nanostructure results in the improvement of the soft magnetic properties in comparison with the Fe–M–B (M = Zr, Si, Nb) alloys. For the sample annealed at 923 K for 20 min, the lowest coercive force H_c and the highest effective permeability are obtained.

(2) The GMI ratio $(\Delta Z/Z)_{max}$ shows the maximal value 383% and the maximal sensitivity of $(\Delta Z/Z)$ larger than 0.9% $(\mathrm{A\ m^{-1}})^{-1}$ at $f = 2.5$ MHz for the $Fe_{84}Zr_{3.5}Nb_{3.5}B_8Cu$ ribbon annealed at 923 K for 20 min. This GMI effect is superior to those of Co-based amorphous wires, ribbons [2, 4] and the Fe–Zr–B–Cu ribbons [8].

(3) The excellent soft magnetic properties play a main role in the high GMI response. On the other hand, the proper transverse anisotropy with respect to the long direction of ribbons is also necessary to obtain the GMI effect.

Acknowledgments

This work was supported by the National Natural Science Foundation of China (59671011) and the State Key Laboratory of Magnetism, Institute of Physics, Chinese Academy of Science and partially by the research item of the Science Commission of Shandong Province, People's Republic of China.

References

[1] Mohri K, Panina L V, Vchiyama T, Bushida K and Noda M 1995 *IEEE Trans. Magn.* **31** 1266
[2] Mohri K, Kawashima K, Yoshida Y and Panina L V 1992 *IEEE Trans. Magn.* **28** 3150
[3] Mohri K, Kawashima K, Kohzawa T and Yoshida Y 1992 *IEEE Trans. Magn.* **29** 3150
[4] Panina L V and Mohri K 1994 *Appl. Phys. Lett.* **65** 1189
[5] Guo H Q, Chen C, Li M, Zhao T Y, Luan K Z, Shen B G, Liu Y H, Zhao J G, Mei L M and Kronmüller H 1997 *Mater. Sci. Eng.* A **226–228** 550
[6] Guo H Q, Kronmüller H, Dragon T, Chen C and Shen B G 1998 *J. Appl. Phys.* **84** 5673
[7] He J, Guo H Q, Shen B G, He K Y and Hu J F 1999 *Acta. Phys. Sin.* **8** 208
[8] He J, Guo H Q, Shen B G, He K Y and Kronmüller H 1999 *J. Appl. Phys.* at press
[9] Sommer R L and Chien C L 1995 *Appl. Phys. Lett.* **67** 3346
[10] Makino A, Hatanai T, Yoshida S, Hasegana N, Inoue A and Masumoto T 1996 *Sci. Rep. RITU* A **42** 121
[11] Herzer G 1989 *IEEE Trans. Magn.* **25** 3327
[12] Suzuki K, Makino A, Kataoka N, Inoue A and Masamoto T 1991 *Mater. Trans. JIM* **32** 93
[13] Panina L V, Mohri K, Uchiyama T and Noda M 1995 *IEEE Trans. Magn.* **31** 1249
[14] Jackson J D 1975 *Classical Electrodynamics* (New York: Wiley)
[15] Machado F L A and Rezende S M 1996 *J. Appl. Phys.* **79** 6558